HHS Public Access

Author manuscript

Magn Reson Med. Author manuscript; available in PMC 2023 May 01.

Published in final edited form as:

Magn Reson Med. 2022 May ; 87(5): 2372–2379. doi:10.1002/mrm.29121.

Three-dimensional reduced field-of-view imaging (3D-rFOVI)

Kaibao Sun[1], **Zheng Zhong**[1,2], **Guangyu Dan**[1,2], **Muge Karaman**[1,2], **Qingfei Luo**[1], **Xiaohong Joe Zhou**[1,2,3,*]

[1]Center for Magnetic Resonance Research, University of Illinois at Chicago, Chicago, IL, United States

[2]Department of Biomedical Engineering, University of Illinois at Chicago, Chicago, IL, United States

[3]Departments of Radiology and Neurosurgery, University of Illinois College of Medicine at Chicago, Chicago, IL, United States

Abstract

Purpose: This study aimed at developing a three-dimensional reduced field-of-view imaging (3D-rFOVI) technique using a 2D RF pulse, and demonstrating its ability to achieve isotropic high spatial resolution and reduced image distortion in echo planar imaging (EPI).

Methods: The proposed 3D-rFOVI technique takes advantage of a 2D RF pulse to excite a slab along the conventional slice-selection direction (i.e., z-direction) while limiting the spatial extent along the phase-encoded direction (i.e., y-direction) within the slab. The slab is phase-encoded in both through-slab and in-slab phase-encoded directions. The 3D-rFOVI technique was implemented at 3 Tesla in gradient-echo and spin-echo EPI pulse sequences for functional MRI (fMRI) and diffusion-weighted imaging (DWI), respectively. 3D-rFOVI experiments were performed on a phantom and human brain to illustrate image distortion reduction, as well as isotropic high spatial resolution, in comparison with 3D full-FOV imaging.

Results: In both the phantom and the human brain, image voxel dislocation was substantially reduced by 3D-rFOVI when compared with full-FOV imaging. In the fMRI experiment with visual stimulation, 3D isotropic spatial resolution of ($2\times2\times2$ mm^3) was achieved with an adequate signal-to-noise ratio (81.5) and BOLD contrast (2.5%). In the DWI experiment, diffusion-weighted brain images with an isotropic resolution of ($1\times1\times1$ mm^3) was obtained without appreciable image distortion.

Conclusion: This study indicates that 3D-rFOVI is a viable approach to 3D neuroimaging over a zoomed region.

Keywords

3D imaging; reduced FOV; 2D RF pulse; isotropic resolution; fMRI; DWI; EPI

[*]Address correspondence to: Xiaohong Joe Zhou, PhD; xjzhou@uic.edu; Phone: 312-413-3979; Fax: 312-355-1637, Center for Magnetic Resonance Research, University of Illinois at Chicago, 2242 West Harrison Street, Suite 103, M/C 831 Chicago, IL 60612.

The work was presented in part at the 29th Annual Meeting of the ISMRM in May of 2021 (Abstract No. 4193).

Introduction:

Echo planar imaging (EPI) has been widely used in functional magnetic resonance imaging (fMRI) and diffusion-weighted imaging (DWI). Its single-shot capability provides high temporal resolution and resiliency to subject motion [1]. However, both gradient-echo EPI (GRE-EPI) and spin-echo EPI (SE-EPI) suffer from geometric distortion and spatial shifts (collectively called spatial dislocation thereafter) caused by various off-resonance effects, such as magnetic susceptibility variations, eddy currents, chemical shifts, concomitant magnetic fields, and bulk B_0-field inhomogeneities [2–5]. The amount of spatial dislocation Δd is given by $\Delta\, d = \frac{2\pi\, \Delta\, f}{BW \bullet\, \Delta\, k}$, where Δf is the amount of off-resonance in Hertz, Δk is the k-space sampling interval, and BW is the sampling bandwidth. Along the phase-encoded direction, BW is inversely related to the inter-echo spacing (T_{esp}) of EPI, and thus is substantially narrower (e.g., ~ 1 kHz) than the bandwidth along the readout direction, leading to exacerbated spatial dislocation.

To mitigate this problem, Δk can be increased, as widely employed in parallel imaging. Another approach is to reduce the field of view (FOV) along the phase-encoded direction using a two-dimensional (2D) RF pulse [6–10], because Δk is inversely proportional to FOV. Imaging with a reduced FOV (rFOV) can also produce a higher in-plane spatial resolution provided that the matrix size is retained. Because of these benefits, rFOV imaging has been increasingly used, particularly in DWI over a focal region, such as the brain stem [10]. Presently, rFOV imaging has been limited to 2D multi-slice applications. Although several elegant methods have been developed to increase the robustness of 2D multi-slice rFOV imaging without being subject to the RF side-band perturbation [8–11], the 2D multi-slice approach has generic drawbacks including compromised slice profile and inferior through-plane spatial resolution that leads to highly anisotropic voxels. These issues can be effectively addressed in three-dimensional (3D) imaging.

The goal of this work is to extend the benefits of rFOV imaging from 2D to 3D to overcome the limitations associated with 2D multi-slice rFOV imaging. We herein describe a 3D reduced field-of-view imaging (3D-rFOVI) method that uses a 2D RF pulse to excite a slab, followed by phase-encoding along the slab direction. The resulting 3D zoomed images with isotropic high spatial resolution and reduced geometric distortion are demonstrated in fMRI and DWI applications in the human brain.

Methods:

3D-rFOVI:

Unlike conventional 2D rFOV imaging where a 2D RF pulse is repetitively applied slice-by-slice, 3D-rFOVI uses a 2D RF pulse to excite a rFOV slab along the conventional slice-selection direction while limiting the spatial extent along the phase-encoded direction within the slab (Figure 1A). Along the through-slab direction, a stepping phase-encoding gradient is applied to provide spatial encoding over a zoomed 3D volume. This approach can result in isotropic high spatial resolution while reducing off-resonance effects that cause image spatial dislocation and signal void [12]. Following the 2D RF excitation and

through-slab phase-encoding, an EPI readout is applied, forming a 3D-rFOV gradient-echo EPI (3D-rFOV GRE-EPI) sequence that can be used for fMRI. Alternatively, an optional slab-selective 180° refocusing pulse can be applied prior to the EPI readout, resulting in a 3D-rFOV spin-echo EPI (3D-rFOV SE-EPI) sequence. Further incorporation of a Stejskal-Tanner gradient enables the 3D-rFOV SE-EPI sequence for DWI applications.

RF pulse and pulse sequence design:

A 2D RF pulse was designed by employing a fly-back EPI-like excitation k-space trajectory to avoid Nyquist ghosts [9,10]. Discrete sampling of excitation k-space along the blipped gradient direction resulted in periodic replicates (or side bands) of the excitation profile (or main band). The separation between the main band and the first side band (ΔS) is the inverse of the excitation k-space sampling interval (Δk_e), which can be expressed as:

$$\Delta S = \frac{1}{\Delta k_e} = \frac{(N-1) \cdot \Delta S_{PE}}{T_{PE} \cdot BW_{PE}}$$

where N is the number of sub-pulses, ΔS_{PE} is the width of excitation band along the phase-encoded direction (i.e., y-direction), and T_{PE} and BW_{PE} are the duration and bandwidth of the envelope RF pulse, respectively. In our design, the main band was used to excite a limited 3D region of interest, while the side bands were positioned outside the imaged object by employing eleven sub-pulses each with a time-bandwidth product (TBP) of 3.01. The amplitude of these sub-pulses was modulated by an envelope RF pulse whose TBP was 3.53 and pulse width was 14.7 ms (Figure 1C). With these parameters, ΔS was approximately $2.8 \times \Delta S_{PE}$. Both the sub-pulses and the envelope pulse were designed using a Shinnar-Le-Roux algorithm with a linear phase and projected ripples of 1% in and out of the slab [13]. The EPI bipolar gradient waveform (i.e., G_z gradient in Figure 1C) concurrent with the 2D RF pulse was designed by minimizing the duration (0.24 ms) of the even (or fly-back) gradient lobes using a triangular waveform. The duration (1.13 ms) of the odd gradient lobes was stretched to take advantage of the time saved by compressing the even gradient lobes. The corresponding RF pulses were also stretched in pulse width accordingly while their amplitudes reduced [1]. Following the 2D RF pulse, a phase-encoding gradient was applied in the slab-selective direction to achieve 3D spatial encoding. The 2D RF pulse with 3D spatial encoding was incorporated into a T2*-weighted GRE-EPI and a diffusion-weighted SE-EPI pulse sequence for experimental demonstrations. Fat suppression was achieved by a frequency-selective saturation pulse prior to the 2D RF pulse.

Experiments:

The T2*-weighted GRE-EPI and diffusion-weighted SE-EPI sequences based on 3D-rFOVI were implemented on a GE MR750 3T scanner (GE Healthcare, Waukesha, Wisconsin, USA). Phantom and human *in vivo* experiments were performed to demonstrate the proposed 3D-rFOVI technique. The human scans were conducted on healthy volunteers with approval from the Institutional Review Board (IRB) and written informed consent from the subjects.

In the first experiment, an American College of Radiology (ACR) phantom was utilized to validate the pulse sequence and its associated 3D image reconstruction. Phantom images from the 3D-rFOV GRE-EPI sequence were acquired with the following parameters: TR/TE = 100/30 ms, volume TR (TR_{vol}) = 2000 ms (where the TR_{vol} is defined as the time taken to acquire a 3D volume), flip angle = 30°, FOV = 256×128 mm^2, slab thickness = 40 mm, acquisition matrix = 128×64×20, and isotropic spatial resolution = 2.0×2.0×2.0 mm^3. The corresponding conventional full-FOV 3D EPI images (FOV = 256×256×40 mm^3, acquisition matrix = 128×128×20) were also acquired for comparison. To establish a reference to assess spatial dislocations, additional images were obtained using a conventional 3D fast SPGR sequence (TR/TE = 5.1/1.8 ms, flip angle = 10°, FOV = 256×256×40 mm^3, and acquisition matrix = 128×128×20). To quantify the geometric distortion, a horizontal line in the SPGR image (red arrows in Figure 2) was chosen as a reference, and the spatial shift between the end and the midpoint of the line along the phase-encoded direction was calculated and compared between the full-FOV and rFOV GRE-EPI images.

In the second experiment, human brain was imaged using a 32-channel head coil (Nova Medical, Inc., Wilmington, Massachusetts, USA) with the same protocol described above. Geometric distortion and image signal-to-noise ratio (SNR) in the visual cortex area were compared between the full-FOV and rFOV GRE-EPI brain images. The SNR was calculated by using signal intensity in the occipital lobe divided by the average of background standard deviations over four regions (each with an area of about 200 mm^2) selected at the corners of the image to avoid residual ghosting artifacts.

The third experiment aimed at demonstrating the 3D-rFOV GRE-EPI sequence for fMRI with visual stimulation. The imaging parameters were: TR/TE = 100/30 ms, TR_{vol} = 2000 ms, number of volumes = 120, flip angle = 30°, FOV = 200×100 mm^2, slab thickness = 40 mm, acquisition matrix = 100×50×20, and isotropic spatial resolution = 2.0×2.0×2.0 mm^3. Visual stimulation was delivered using a commercial system (SensaVue, Invivo Corporation, Gainesville, Florida, USA) with a dark-gray and light-gray checkboard pattern flashing at 8 Hz. Our block-design paradigm contained five 48 s blocks, each with a 24 s rest period and a 24 s stimulation. The total acquisition time was 4 min. A healthy human subject (32-year-old male) was asked to fixate on the cross-hair presented at the center of visual field during the experiment. All data were analyzed using SPM8 on MATLAB 2012b (The MathWorks, Inc., Natick, Massachusetts, USA). Motion correction and spatial smooth (FWHM = 6 mm) were applied to magnitude images, followed by statistical analyses using a general linear model for activation detection with a *P*-value threshold (FWE corrected) of < 0.05.

In the fourth experiment, 3D zoomed diffusion-weighted brain images were acquired from the mid-brain region of healthy human subjects using a 3D-rFOV SE-EPI sequence. The key acquisition parameters were: TR/TE = 4000/72 ms, FOV = 160×80 mm^2, slab thickness = 40 mm, matrix size = 160×80×40, isotropic spatial resolution = 1×1×1 mm^3, diffusion gradient direction = anterior-posterior, $b_{NEX} = 0_1$ and 1000_3 s/mm^2 (where the subscripts indicate the number of averages), and scan time = 10 min and 44 s. Maps of apparent diffusion coefficient (ADC) were obtained from the images acquired at the two b-values using custom software in MATLAB with a mono-exponential model. Regions of interest

(ROIs) were drawn bilaterally at the frontotemporal area and corona radiata to calculate the average ADC values in the gray and white matters, respectively.

Results:

Phantom results:

Figure 2 displays images from the first experiment, including the results from the conventional 3D SPGR sequence (Figure 2A), the 3D EPI sequence with a full FOV (Figure 2B), and the 3D-rFOVI sequence (Figure 2C). For each sequence, a representative image corresponding to slice No. 5 of the ACR phantom was selected from the 3D volumetric dataset. The spatial dislocation was measured by the shift along the vertical phase-encoded direction between the end and the midpoint of the third horizonal reference line, as indicated by the red arrows in Figure 2. Compared with the 3D SPGR reference image (Figure 2A), the spatial dislocation was 8 and 4 pixels in the full-FOV (Figure 2B) and rFOV GRE-EPI images (Figure 2C), respectively. In general, the 3D-rFOV GRE-EPI image exhibited much less geometric distortion than the 3D full-FOV GRE-EPI image when the conventional SPGR image was used as a reference.

Human imaging results:

Representative 3D-rFOV GRE-EPI images ($2\times2\times2$ mm^3 isotropic voxel size) selected from a 3D volume of the human brain (second experiment) are shown in Figure 3. Reduced geometric distortion was observed in the 3D rFOV images when compared with 3D full-FOV images. Quantitative measurement of SNR in the region of visual cortex revealed an approximately 30% reduction in the 3D rFOV image (SNR = 81.5) compared with the 3D full-FOV image (SNR = 117.6). Results from the third experiment on fMRI are displayed in Figure 4 where eight contiguous activation maps from the 3D-rFOV GRE-EPI acquisition are overlaid on the corresponding baseline images. fMRI activations were observed in the visual cortex, as expected. The time evolution of BOLD signal change (approximately 2.5%, obtained from the average signal) in the activated visual cortex area is illustrated in Figure 4B. Figure 5 shows a set of 3D zoomed diffusion-weighted brain images acquired with the 3D-rFOV SE-EPI sequence. Three-dimensional diffusion-weighted images with isotropic high spatial resolution ($1\times1\times1$ mm^3) was achieved without appreciable image distortion. The ADC maps calculated from the images with two b-values (bottom row in Figure 5) revealed average ADC values of 0.96 ± 0.12 $\mu m^2/ms$ and 0.85 ± 0.21 $\mu m^2/ms$ in the representative gray (frontotemporal area) and white (corona radiata) matters, respectively, which are consistent with the literature values (gray matter: 0.78–1.09 $\mu m^2/ms$ [14]; white matter: 0.60–1.05 $\mu m^2/ms$ [15]).

Discussions:

Our study demonstrated a 3D-rFOVI technique, which enabled focused 3D imaging in a larger object. By combining the slab-selective capability of a 2D RF pulse with 3D spatial encoding, 3D-rFOVI achieved isotropic high spatial resolution and reduced geometric distortion in phantom and human brain images with specific demonstrations for anatomic imaging, fMRI, and DWI applications.

It has been shown that reducing FOV is an effective strategy to achieve high spatial resolution and mitigate geometric distortion. This approach has been well demonstrated in an increasing number of applications using 2D multi-slice imaging [10,16–18]. However, achieving 3D isotropic resolution remains challenging as the 2D RF pulses employed in 2D rFOV imaging typically produce a much lower spatial resolution through-plane than in-plane, often due to the constraints of the RF pulse and the gradient [1]. By employing 2D slab-excitation (i.e., intentionally making the through-plane resolution worse) followed by through-plane phase encoding, we have overcome this limitation and achieved 3D isotropic spatial resolution. Because a thin slice is no longer pursued in the 2D RF pulse design for 3D rFOVI, the pulse width of the sub-pulses, gradient slew rate, and gradient amplitude are all relaxed. The shortened RF pulse, for example, provided more flexibility in selecting TE for fMRI studies and minimizing TE for DWI.

Similar to conventional 2D rFOV imaging, 3D-rFOVI also relies on a 2D RF pulse, and as such is subject to periodic side-band excitations arising from discrete sampling. In accordance with the properties of Fourier transform, the separation between the bands is inversely related to the separation of two adjacent excitation k-space lines (Δk_e). In the fMRI and DWI experiments, Δk_e was designed to be 0.0035 mm^{-1} and 0.0044 mm^{-1}, respectively, which positioned the closest side bands more than 200 mm away along the phase-encoded direction. This design effectively avoided perturbations from the side bands.

3D rFOVI can be achieved using alternative techniques. For example, parallel transmit is a viable approach to 3D inner-volume excitation while maintaining a short duration of multidimensional RF pulses [19]. This method, however, requires expensive hardware and sophisticated RF pulse design strategies that are not commonly available on clinical 3T and 1.5T scanners. A 3D zoomed volume can also be isolated using three RF pulses such as a 90°–180°–180° or 90°–90°–90° pulse train, followed by phase-encoding. Each of the these RF pulses in the pulse train is applied with a gradient along an orthogonal spatial direction, selecting a 3D zoomed volume at the intersection [20,21]. In spin-echo sequences, the number of required RF pulses can be reduced to two for 3D rFOVI because zooming in the readout direction can be accomplished using anti-aliasing filtering. In comparison with the proposed 3D-rFOVI technique, the approach with orthogonal profiles is not subject to periodic side bands arising from discrete excitation k-space sampling, which can be advantageous. However, this approach perturbs spins outside the selected intersection, limiting subsequent selections in other regions when multiple 3D zoomed volumes are desired, such as in 3D multi-slab imaging [22–24]. In addition, the reliance on two or more RF pulses makes the method incompatible with GRE-EPI for neurofunctional imaging. Another approach of achieving 3D rFOVI is outer-volume suppression (OVS) [25]. This technique requires lengthy pre-saturation pulses and is typically subject to imperfect suppression caused by B_0 inhomogeneities and/or B_1 non-uniformity. Incomplete signal suppression from the outer volume can lead to aliasing artifacts, interfering with the signals from the focused region of interest. The 3D-rFOVI approach employed in this study avoids the aforementioned problems.

The fly-back EPI-like excitation k-space trajectory employed in our 2D RF pulse design provides robustness against gradient infidelities (particularly those caused by eddy currents)

than bidirectional EPI-like gradient waveform [26]. In addition, the fly-back k-space trajectory allows 1D RF pulses (sub-pulses and their envelope RF pulse) to be designed separately, which provides independent control of two out of the three dimensions of the excited volume compared with a spiral trajectory [27,28]. A major drawback is that the fly-back EPI-like excitation k-space trajectory can lead to an increased duration of the 2D RF pulse, lengthening the minimum echo time and repetition time. Other 2D RF pulse design strategies also exist, such as those using a discretized matrix [26]. The alternative 2D RF design methods should be investigated in future studies.

The benefits of using 3D-rFOVI are expected to be greater at a higher magnetic field where the need for image distortion reduction is more prominent due to the increased off-resonance effects and where the improved SNR can better support high isotropic spatial resolution. In principle, the former issue can also be mitigated by incorporating parallel imaging. However, the limited RF coil sensitivity variation over a reduced FOV will likely make parallel imaging reconstruction very challenging. Other methods to reduce image distortion have also been reported, including magnetization preparation followed by segmented SPGR readout (instead of EPI) [29–31]. The latter issue is particularly important for 3D-rFOVI because of an intrinsic loss in SNR as a result of the reduced sampling in k-space as well as a smaller voxel size. As shown in the second experiment, the SNR in the 3D-rFOV GRE-EPI images was reduced by about 30% compared to 3D full-FOV GRE-EPI images. This SNR reduction was consistent with the fact that only one half of k-space data were acquired in the 3D-rFOV scan as compared to those in the full FOV acquisition (Theoretically, the SNR is reduced by $\left(1-\frac{1}{\sqrt{2}}\right)\times 100\%$, or about 29%, which is consistent with our experimental observations). At 3 Tesla, the decreased SNR in 3D-rFOVI may require more signal averaging, as we showed in the DWI experiments. In addition, the SNR can be reduced further when a small flip angle is used in the 3D-rFOV GRE-EPI sequences to avoid signal saturation in the fMRI experiments. Our analysis showed that up to 25% reduction in SNR could occur when compared to the scenario of using a 90° flip angle. To improve SNR efficiency and increase spatial coverage, a 3D multi-slab technique (a hybrid between 2D and 3D imaging) [22–24], may be incorporated into 3D-rFOVI in future studies. Another limitation of the study is that the FOV reduction was demonstrated only along the phase-encoded and slab-selection directions. Limiting the FOV along the readout direction can be readily achieved by taking advantage of the anti-aliasing filters that are widely implemented on commercial MRI scanners [1].

Conclusions:

We have demonstrated a novel technique, 3D-rFOVI, to enable 3D imaging over a zoomed region. The 3D-rFOVI technique takes advantage of the spatial response of a 2D RF pulse to simultaneously limit the spatial extents along the phase-encoded direction (i.e., y-direction) and the conventional “slice-selection” direction (i.e., z-direction). The technique has been demonstrated in fMRI and DWI on the human brain, where substantial reduction in geometric distortion was achieved together with isotropic high spatial resolution of (2 mm)^3 and (1 mm)^3, respectively. These new capabilities are expected to enhance or enable neuroimaging applications and beyond.

Acknowledgements:

This work was supported in part by the National Institutes of Health (5R01EB026716 and 1S10RR028898). The content is solely the responsibility of the authors and does not necessarily represent the official views of the National Institutes of Health. The fMRI studies were supported in part by an award from the University of Illinois at Chicago under the Chancellor's Translational Research Initiative Program. The authors are grateful to Dr. Y. Sui for helpful discussions, technical assistance, and providing the artwork used in Figure 1.

Funding source:

This work was supported in part by grants from the National Institutes of Health (Grant Numbers NIH R01EB026716 and 1S10RR028898).

Data availability statement

The sample data and reconstruction code used in this study will be made available at https://github.com/uic-cmrr-3t/3D-rFOVI from the date of publication. Other relevant image datasets will be released upon request to the corresponding author, subject to local IRB and other regulations.

References:

1. Bernstein MA, King KF, Zhou XJ. Handbook of MRI pulse sequences. In: Amsterdam: Elsevier, Academic Press. ; 2004.
2. Jezzard P, Clare S. Sources of distortion in functional MRI data. Hum Brain Mapp. 1999;8(2–3):80–85. [PubMed: 10524596]
3. Rohde GK, Barnett AS, Basser PJ, Marenco S, Pierpaoli C. Comprehensive approach for correction of motion and distortion in diffusion-weighted MRI. Magn Reson Med. 2004;51(1):103–114. [PubMed: 14705050]
4. Zhou XJ, Du YP, Bernstein MA, Reynolds HG, Maier JK, Polzin JA. Concomitant magnetic-field-induced artifacts in axial echo planar imaging. Magn Reson Med. 1998;39(4):596–605. [PubMed: 9543422]
5. Jezzard P Correction of geometric distortion in fMRI data. Neuroimage. 2012;62:648–651. [PubMed: 21945795]
6. Alley MT, Pauly JM, Sommer FG, Pelc NJ. Angiographic imaging with 2D RF pulses. Magn Reson Med. 1997;37(2):260–267. [PubMed: 9001151]
7. Rieseberg S, Frahm J, Finsterbusch J. Two-dimensional spatially-selective RF excitation pulses in echo-planar imaging. Magn Reson Med. 2002;47(6):1186–1193. [PubMed: 12111965]
8. Saritas EU, Cunningham CH, Lee JH, Han ET, Nishimura DG. DWI of the spinal cord with reduced FOV single-shot EPI. Magn Reson Med. 2008;60(2):468–473. [PubMed: 18666126]
9. Finsterbusch J Fast-spin-echo imaging of inner fields-of-view with 2D-selective RF excitations. J Magn Reson Imaging. 2010;31(6):1530–1537. [PubMed: 20512911]
10. Zhong Z, Merkitch D, Karaman MM, et al. High-spatial-resolution diffusion MRI in Parkinson disease: lateral asymmetry of the substantia nigra. Radiology. 2019;291(1):149–157. [PubMed: 30777809]
11. Banerjee S, Nishimura DG, Shankaranarayanan A, Saritas EU. Reduced field-of-view DWI with robust fat suppression and unrestricted slice coverage using tilted 2D RF excitation. Magn Reson Med. 2016;76(6):1668–1676. [PubMed: 27654126]
12. Cordes D, Turski PA, Sorenson JA. Compensation of susceptibility-induced signal loss in echo-planar imaging for functional applications. Magn Reson Imaging. 2000;18(9):1055–1068. [PubMed: 11118760]
13. Pauly J, Le Roux P, Nishimura D, Macovski A. Parameter relations for the Shinnar-Le Roux selective excitation pulse design algorithm. IEEE Trans Med Imaging. 1991;10(1):53–65. [PubMed: 18222800]

14. Helenius J, Soinne L, Perkiö J, et al. Diffusion-weighted MR imaging in normal human brains in various age groups. Am J Neuroradiol. 2002;23(2):194–199. [PubMed: 11847041]
15. Sener RN. Diffusion MRI: Apparent diffusion coefficient (ADC) values in the normal brain and a classification of brain disorders based on ADC values. Comput Med Imaging Graph. 2001;25(4):299–326. [PubMed: 11356324]
16. Islam H, Glover GH. Reduced field of view imaging using a static second-order gradient for functional MRI applications. Magn Reson Med. 2016;75(2):817–822. [PubMed: 25809723]
17. Vidiri A, Minosse S, Piludu F, et al. Feasibility study of reduced field of view diffusion-weighted magnetic resonance imaging in head and neck tumors. Acta radiol. 2017;58(3):292–300. [PubMed: 27287402]
18. Finsterbusch J Functional neuroimaging of inner fields-of-view with 2D-selective RF excitations. Magn Reson Imaging. 2013;31(7):1228–1235. [PubMed: 23602726]
19. Katscher U, Börnert P, Leussler C, Van den Brink JS. Transmit SENSE. Magn Reson Med. 2003;49(1):144–150. [PubMed: 12509830]
20. Feinberg DA, Hoenninger JC, Crooks LE, Kaufman L, Watts JC, Arakawa M. Inner volume MR imaging: technical concepts and their application. Radiology. 1985;156(3):743–747. [PubMed: 4023236]
21. Yacoub E, Duong TQ, Van De Moortele PF, et al. Spin-echo fMRI in humans using high spatial resolutions and high magnetic fields. Magn Reson Med. 2003;49(4):655–664. [PubMed: 12652536]
22. Posse S, Ackley E, Mutihac R, et al. Enhancement of temporal resolution and BOLD sensitivity in real-time fMRI using multi-slab echo-volumar imaging. Neuroimage. 2012;61(1):115–130. [PubMed: 22398395]
23. Chang HC, Sundman M, Petit L, et al. Human brain diffusion tensor imaging at submillimeter isotropic resolution on a 3Tesla clinical MRI scanner. Neuroimage. 2015;118:667–675. [PubMed: 26072250]
24. Holdsworth SJ, O'Halloran R, Setsompop K. The quest for high spatial resolution diffusion-weighted imaging of the human brain in vivo. NMR Biomed. 2019;32:e4056. [PubMed: 30730591]
25. Fleysher L, Fleysher R, Heeger DJ, Inati S. High resolution fMRI using a 3D mult-shot EPI sequence . In: Proceedings of the 13th Annual Meeting of ISMRM, Florida, USA. ; 2005:2685.
26. Schulte RF, Wiesinger F. Direct design of 2D RF pulses using matrix inversion. J Magn Reson. 2013;235:115–120. [PubMed: 24013595]
27. Nunes RG, Ferrazzi G, Price AN, et al. Inner-volume echo volumar imaging (IVEVI) for robust fetal brain imaging. Magn Reson Med. 2018;80(1):279–285. [PubMed: 29115686]
28. van der Zwaag W, Reynaud O, Narsude M, Gallichan D, Marques JP. High spatio-temporal resolution in functional MRI with 3D echo planar imaging using cylindrical excitation and a CAIPIRINHA undersampling pattern. Magn Reson Med. 2018;79(5):2589–2596. [PubMed: 28905414]
29. Yuan J, Hu Y, Menini A, et al. Near-silent distortionless DWI using magnetization-prepared RUFIS. Magn Reson Med. 2020;84(1):170–181. [PubMed: 31782557]
30. Solana AB, Menini A, Sacolick LI, Hehn N, Wiesinger F. Quiet and distortion-free, whole brain BOLD fMRI using T2-prepared RUFIS. Magn Reson Med. 2016;75(4):1402–1412. [PubMed: 25962633]
31. Hua J, Qin Q, Van Zijl PCM, Pekar JJ, Jones CK. Whole-brain three-dimensional T2-weighted BOLD functional magnetic resonance imaging at 7 Tesla. Magn Reson Med. 2014;72(6):1530–1540. [PubMed: 24338901]

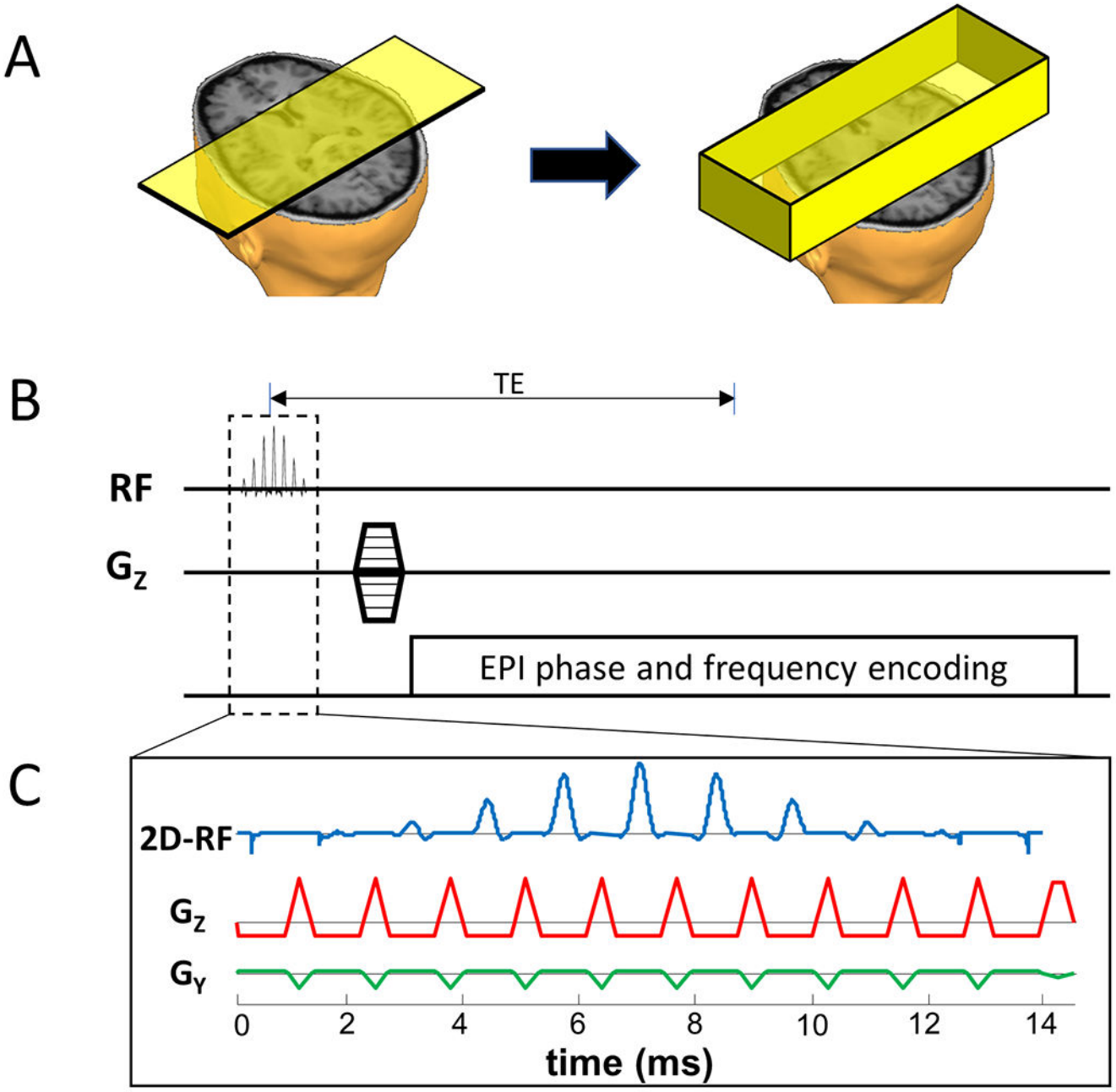

Figure 1:
(A): A schematic to illustrate 3D rFOVI by replacing slice selection with slab selection using a 2D RF pulse in (C), followed by through-slab phase-encoding as shown in (B). (B): A conceptual 3D rFOVI sequence with phase-encoding gradient along the slab direction. (C): Details of the 2D RF excitation pulse with a fly-back EPI excitation k-space trajectory to avoid the issues associated with Nyquist ghosts.

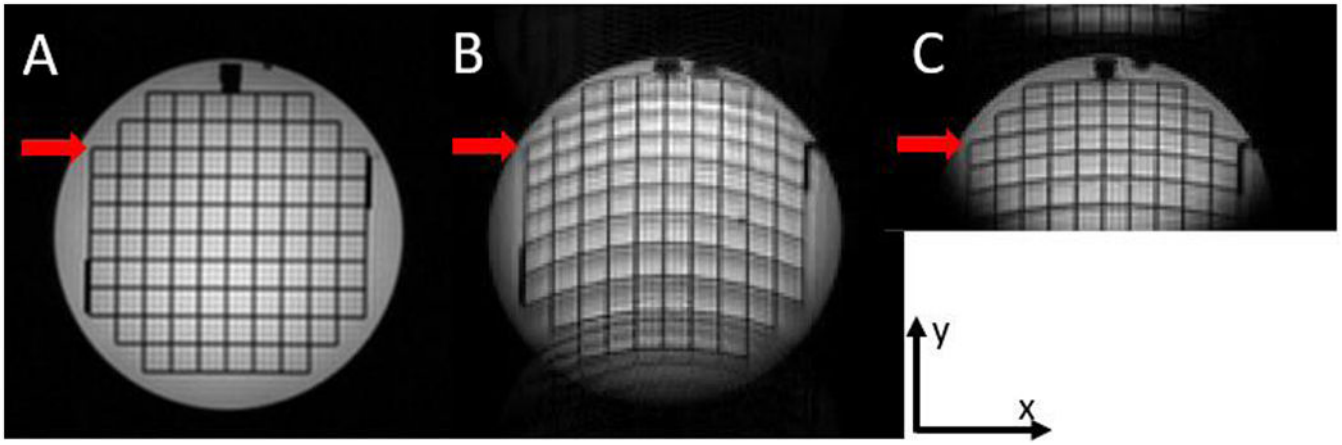

Figure 2:

Representative images of a slice selected from 3D datasets of the ACR phantom acquired using three different sequences: (A) a 3D SPGR sequence, (B) a 3D GRE-EPI sequence with a full FOV, and (C) the 3D-rFOVI sequence with GRE-EPI as shown in Figure 1. Compared to the reference image in (A), the image in (B) exhibited excessive image distortion. In contrast, image distortion was substantially reduced in (C). The distances along the phase-encoded direction (i.e., y-direction) between the end and the midpoint of the third horizontal line (red arrows) were 8 pixels in (B) and 4 pixels in (C). The aliasing artifact in (C) was caused by a slight mismatch between the prescribed rFOV and the 2D RF excitation profile.

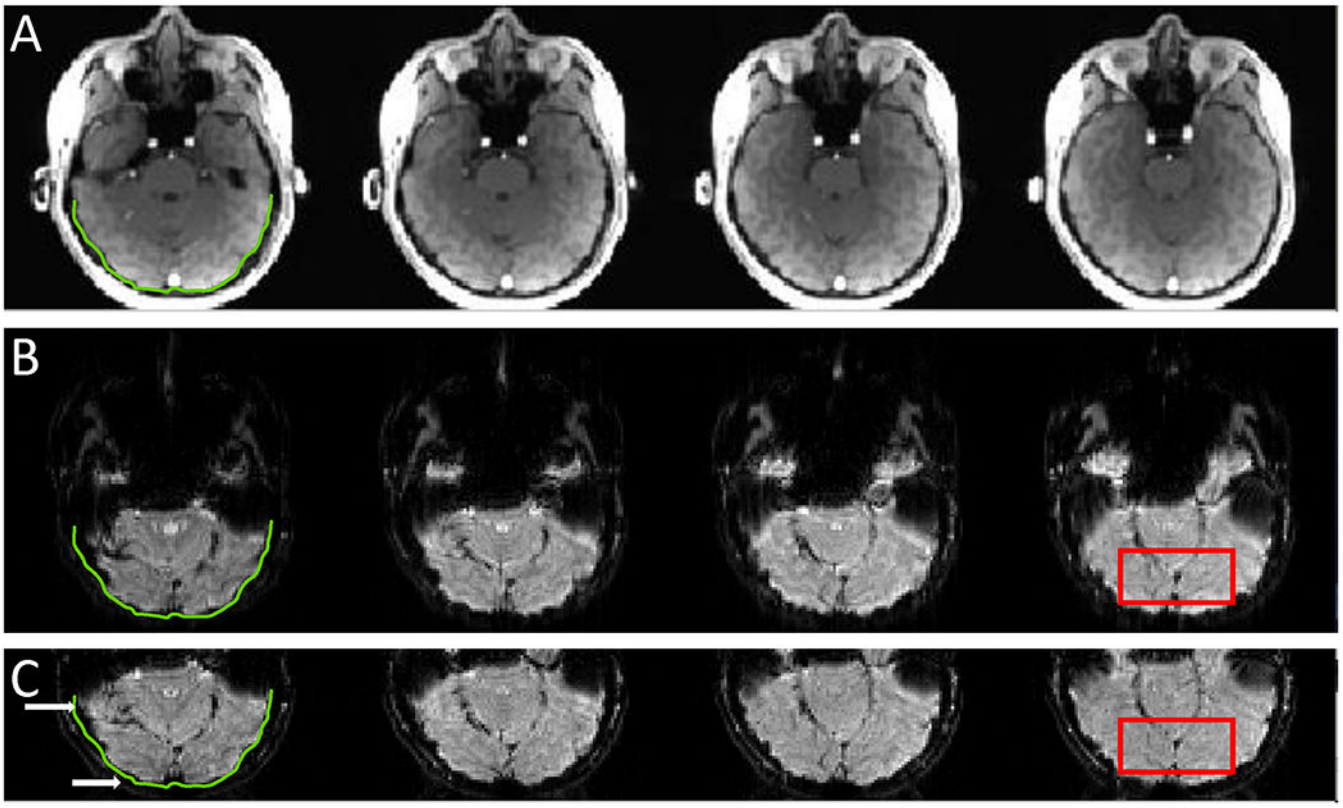

Figure 3:
Four representative contiguous slices selected from 3D datasets of human visual cortex acquired using three different sequences: (A) a 3D SPGR sequence, (B) a 3D GRE-EPI with a full FOV, and (C) the 3D-rFOV GRE-EPI sequence. The green contour outlines the edge of the brain parenchyma in the SPGR image in (A), and is used as a reference. Compared to the full-FOV images in (B), the image in (C) exhibited less image distortion (white arrows). The SNRs measured in the region of visual cortex (red frames) in (B) and (C) were 117.6 and 81.5, respectively.

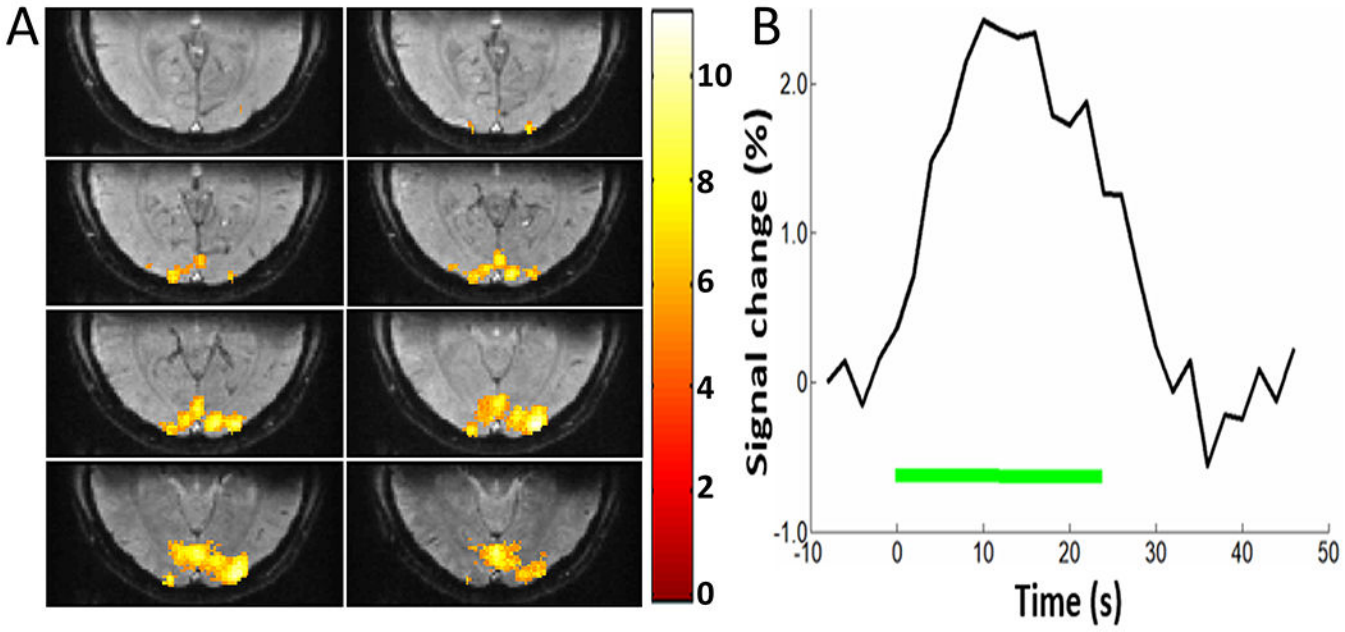

Figure 4:

(A): Eight contiguous visual fMRI activation maps, selected from the 3D volume, overlaid onto the baseline images acquired with 3D-rFOV GRE-EPI. (B): The time course over 48 s illustrates the activation with a BOLD signal change of approximately 2.5%. The green bar represents the time period for the visual stimulus, which was 24 s.

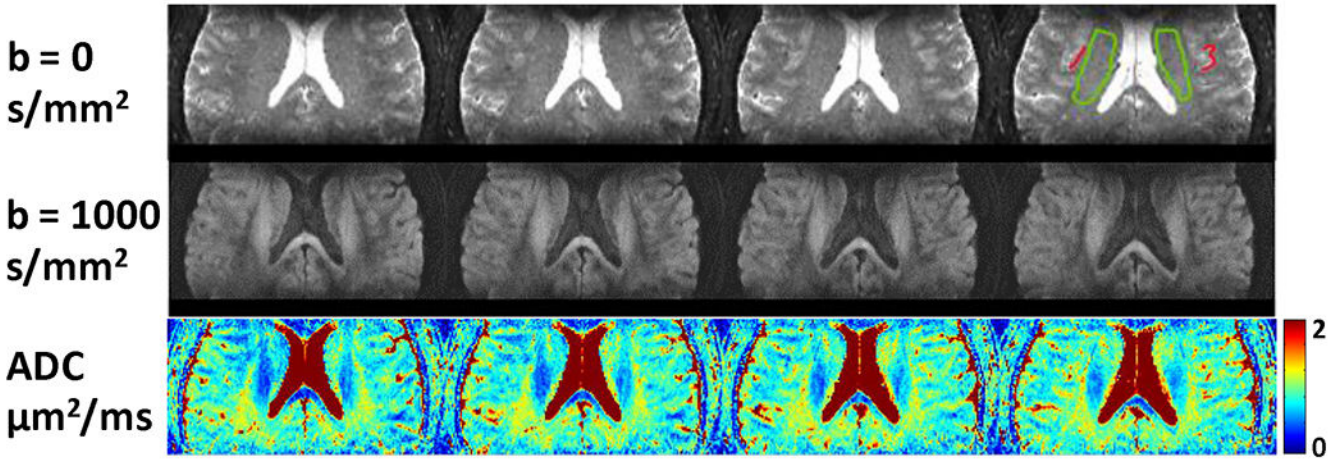

Figure 5:

Representative T2- (1st row) and diffusion-weighted (2nd row) 3D brain images acquired using 3D-rFOV SE-EPI on a healthy human brain (25-year-old male), together with the corresponding ADC maps (3rd row). Using 3D-rFOVI, three-dimensional isotropic high spatial resolution (1×1×1 mm^3) was achieved without appreciable image distortion. Bilateral ROIs were drawn at the frontotemporal area (red) and corona radiata (green) to calculate the average ADC values of representative gray and white matters, respectively. The corresponding ADC values were 0.96 ± 0.12 μm^2/ms for the gray matter and 0.85 ± 0.21 μm^2/ms for the white matter.